Atomic and electronic characterization of the $a[100]$ dislocation core in $SrTiO_3$

Zaoli Zhang, Wilfried Sigle, and Manfred Rühle
Max-Planck-Institut für Metallforschung, Heisenbergstraße 3, D-70569 Stuttgart, Germany
(Received 4 February 2002; revised manuscript received 29 April 2002; published 17 September 2002)

The structure and chemistry of the $a[100]$ edge-dislocation core in $SrTiO_3$ was investigated by high-resolution transmission electron microscopy and electron-energy-loss spectroscopy. The dislocation core is found to be compact, with only a slight dissociation on the {100} plane. This indicates that the {100} antiphase boundary energy is high. The shapes of the Ti-$L_{2,3}$ edge and the oxygen K edge slightly change in the dislocation core with respect to the bulk. In the core, the crystal-field splitting is decreased by 0.2–0.4 eV while the L_3/L_2, the Ti/O, and the e_g/t_{2g} intensity ratios are increased. Structure models are proposed that exhibit a charged, oxygen-deficient dislocation core. This is in good accord with previous plasticity experiments and impedance spectroscopy measurements.

DOI: 10.1103/PhysRevB.66.094108 PACS number(s): 61.72.Lk, 82.80.Pv, 87.64.Ee, 61.72.Ff

I. INTRODUCTION

Oxide ceramics with a perovskite structure have manifold applications, for example as varistors,[1] ferroelectrics,[2] grain boundary layer capacitors, substrates for superconductors[3] and oxygen sensors. $SrTiO_3$ is most important as a dielectric material in capacitors. Here grain boundaries play a crucial role. Among the various types of grain boundaries, low-angle grain boundaries have only scarcely been studied up to now. Such boundaries are composed of isolated dislocations. Recently, low-angle grain boundaries were found to strongly block the transport of charge due to the depletion of electron holes (and oxygen vacancies).[4] From the measured space-charge potential at the grain boundary a charge equivalent to 0.93 elementary charges per unit cell length along the dislocation core was deduced. However, it is not clear up to now whether the charge is solely confined in the very dislocation core or spread uniformly over the grain boundary.

Dislocations also play a surprising role in the plasticity of $SrTiO_3$. In a recent study[5,6] it was shown that the temperature dependence of the critical resolved shear stress of dislocations is weak (comparable to that of many fcc metals), even down to liquid-nitrogen temperature. At elevated temperatures a ductile-to-brittle-to-ductile transition was observed. A model was proposed based on different dislocation core structures at low and high temperatures.

In this paper, dislocation cores in a 5° ⟨100⟩ tilt grain boundary of a $SrTiO_3$ bicrystal were analyzed. Since strong lattice distortions and changes of the electronic structure are comprised to only a few atom layers of the grain boundary, it is most desirable to understand the structure and chemistry at the atomic level. The atomistic structure is studied by high-resolution transmission electron microscopy (HRTEM), and the local electronic structure and chemical composition is resolved by electron-energy-loss spectroscopy (EELS). This has been demonstrated for interfaces,[7–10] grain boundaries,[11] and dislocation cores.[12,13] The chemical composition is determined from the area under specific ionization edges whereas the energy-loss near-edge structure (ELNES) carries information about the electronic structure and coordination of the atoms.

II. EXPERIMENTAL PROCEDURES

5.4° [001] symmetrical tilt $SrTiO_3$ bicrystals with a nominal Fe concentration of 5×10^{19} cm^{-3} were obtained from Shinkosha Co. Ltd., Tokyo, Japan. The low-angle grain boundary was made by diffusion bonding.[14] The sample size was $10\times10\times0.8$ mm^3, with the grain boundary parallel to the large sample faces.

TEM samples were prepared by grinding, dimpling, polishing and ion milling as the final step.[15] For ion milling an inclination angle of 12° was used. The ion energy was 3 keV in a Gatan Duomill.

HRTEM studies were performed on a JEOL 4000EX microscope operated at 400 kV with a point resolution of 0.175 nm. The sample was oriented precisely parallel to the [001] zone axis which is common to both grains.

For analytical TEM a dedicated scanning TEM (STEM) (VG HB 501 UX, Vacuum Generators) was used. The microscope was operated at 100 keV. It is equipped with a cold field-emission gun, an energy dispersive x-ray spectrometer (Noran), and an electron-energy-loss spectrometer (Gatan UHV ENFINA766). The same specimens were used as in the HRTEM studies. The energy resolution in EELS, as measured by the full width at half maximum of the zero-loss peak, was 0.7 eV. The electron probe size was below 1 nm. The probe currents used were in the range of 0.5–1 nA. Spectra were recorded with a dispersion of 0.1 and 0.2 eV/channel, which allows one to simultaneously acquire the Ti $L_{2,3}$ edge and the O K edge. The energy scale for the EELS spectra was calibrated by setting the low-energy Ti white line to 456 eV. For this reason energy shifts stated below denote *relative* energy shifts. The convergence and collection semi-angles were both 6.5 mrad. All data shown here were corrected for dark current and detector gain variation. The spectrum acquisition and processing were done with the Digital Micrograph 3.6 Spectrum Imaging and EL/P software. The background for each spectrum was subtracted by the fit of a power-law function to the pre-edge background.[16] Hartree-Slater cross sections were used for the quantification. For the Ti L edge a 50-eV energy window was used to fit the theoretical cross section to the experimental data. For the determination of the L_1/L_2 and e_g/t_{2g} intensity ratios (see below

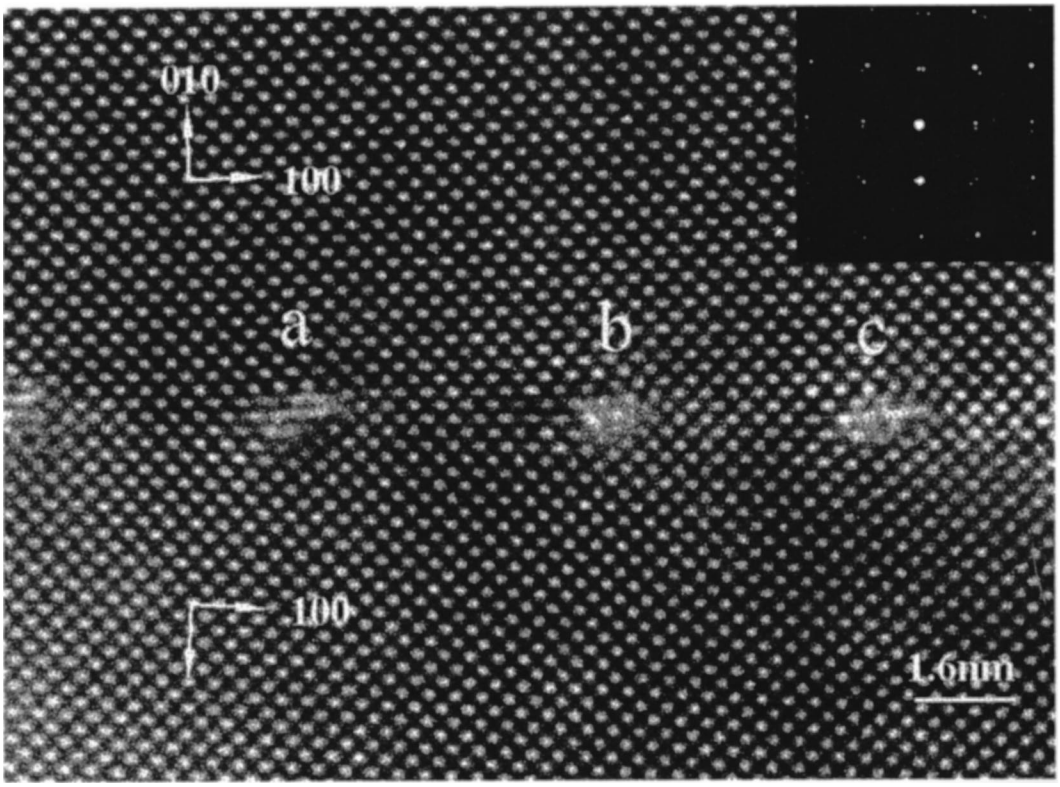

FIG. 1. HRTEM image of the 5.4° [001] symmetrical tilt grain boundary. The inserted diffraction pattern shows double reflections originating from the tilt of the two adjoining crystals. Note the slightly different structure of cores marked *a* and *b*.

and the Appendix) the theoretical Hartree-Slater cross section (exhibiting no white lines) was subtracted from the experimental data. Gaussians were fitted to the remaining white lines, and the areas under the Gaussians were used for the ratio measurements.[17]

Local information from the dislocation core can be obtained directly by placing the electron beam in the center of the core. Owing to the difficulty to locate the very core precisely, we recorded EELS line scans and EELS maps. Furthermore spectra were recorded from a small area containing the dislocation cores.

It has been shown that during ion milling the near-surface region becomes nonstoichiometric.[18] Therefore EELS spectra were not acquired from very thin parts of the specimens (<10 nm) in order to avoid influences from the specimen surface.

III. RESULTS

A. HRTEM

The HRTEM image of the low-angle [001] tilt grain boundary (Fig. 1) shows that the misorientation between the crystals leads to the formation of a regular array of crystal imperfections separated by regions of strained lattice. The misorientation angle can be determined from lattice fringes to be $5.4\pm0.1°$. The pure tilt grain boundary is composed of pure edge dislocations, the average spacing of which can be determined according to Frank's formula: $d_{\mathrm{th}} = |\mathbf{b}|/[2\sin(\theta/2)]$, where θ is the tilt angle and $|\mathbf{b}|$ the modulus of the Burgers vector. For $\theta = 5.4°$ and $|\mathbf{b}| = 0.3905$ nm, d_{th} corresponds to 4.14 nm, which is in excellent agreement with the experimental value of 4.1 ± 0.1 nm deduced from the HRTEM image. A diffraction pattern was inserted in the corner, which shows two $\langle 100\rangle$ patterns that are rotated against each other by 5.4°.

Using the IDIM software package[19] we performed a quantitative comparison of calculated images with the experimental images. From this we obtained a best fit with a defocus value of -75 nm and a specimen thickness of 2 nm. Under these conditions atom columns are imaged with bright contrast.

B. EELS

EELS spectra from the dislocation cores were obtained through the following three modes and then compared with spectra taken from adjacent bulk areas.

1. Line scan measurement

Five EELS spectra were acquired along a line with a total length of about 5.0 nm across the dislocation core (Fig. 2). By comparing images recorded before and after the line scan acquisition, no sample drift could be detected if the acquisition time for each spectrum was equal or less than 2 s [Figs. 2(a) and 2(b)]. Therefore, the third spectrum should represent the information from the dislocation core. The dispersion used was 0.2 eV per channel.

The spectra [Fig. 3(a)] show the four Ti-$L_{2,3}$ white lines and the O-*K* edge. Owing to the short acquisition time the

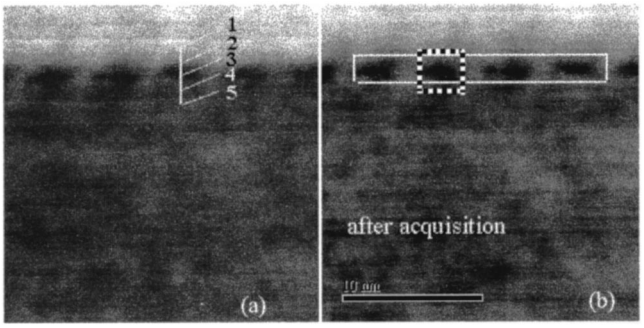

FIG. 2. STEM image before (a) and after (b) acquisition. No specimen drift is visible. Five EELS spectra were recorded along the indicated line in (a). In (b) the sizes of the area measurement (full line) and the mapping (dotted line) are shown.

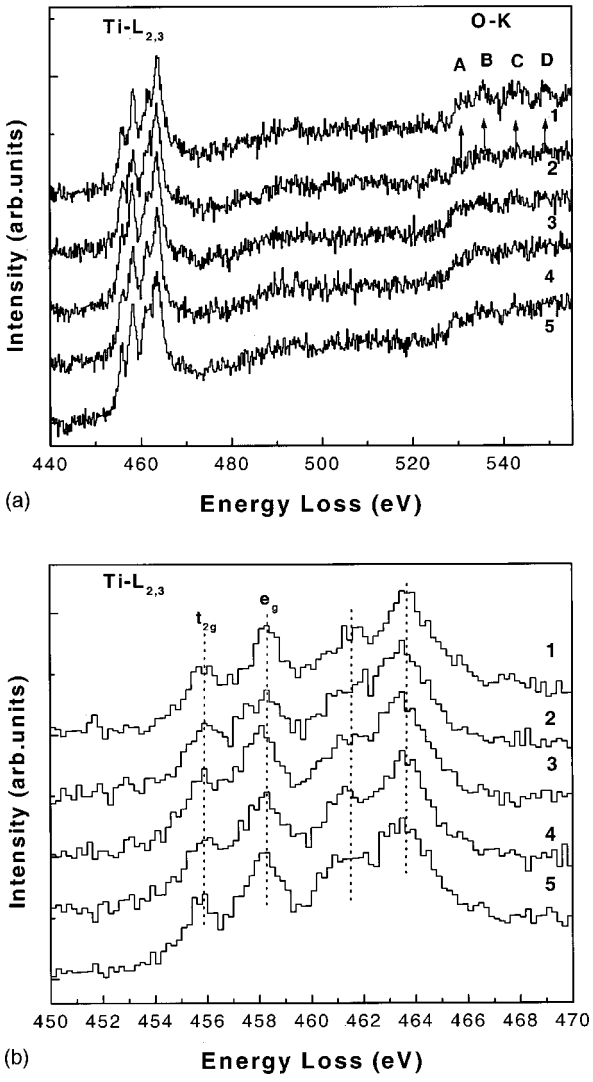

FIG. 3. (a) EELS spectra which were obtained by a line scan across a dislocation core. The separation between subsequent measurements was 1 nm. (b) Enlargement of the Ti-$L_{2,3}$ edge showing a very slight decrease of the crystal-field splitting in spectrum 3.

signal-to-noise ratio (SNR) is low. An enlarged view of the Ti edge is shown in Fig. 3(b). The only recognizable difference between spectrum 3 and the other spectra is a narrowing of the crystal field splitting by one channel, corresponding to 0.2 eV. The Ti/O intensity ratios were extracted at each location. It was found to be higher by $(13\pm9)\%$ in spectrum 3 with respect to the substrate spectra. For the oxygen *K* edge, the characteristic peaks from the bulk (cf. Fig. 8 and the Appendix) are only clearly visible in spectra 1 and 5.

2. Area measurement

EELS spectra were recorded while scanning the beam over a rectangular area of about 1×12 nm^2, containing three dislocation cores as schematically indicated in Fig. 2(b). Such measurements contain a mixture of bulk and dislocation core-specific spectra. The advantage of this method is that long acquisition times can be used. This is because specimen drift can be corrected manually during the measurement since the image and EELS spectra are recorded simultaneously. Spectra from the grain boundary region and from the nearby bulk on either side of the grain boundary were recorded with a dispersion of 0.1 eV per channel. The total acquisition time was 30 s for each spectrum resulting in a much better SNR compared to the line scan spectra.

The Ti-$L_{2,3}$ edge and the O-*K* edge are presented in Fig. 4. Again, only a small change is observed for the grain boundary spectrum with respect to the bulk spectrum. For close inspection, enlarged spectra of the Ti-$L_{2,3}$ edge [Fig. 4(b)] and the O-*K* edge [Fig. 4(c)] are shown. On the grain boundary the intensity of the L_3 e_g peak is decreased, and the separation between the e_g and t_{2g} peaks (crystal field splitting) is reduced by about 0.2 eV as indicated by dotted lines. This corresponds well with the shift observed for the line scan spectra.

The Ti/O ratio was found to be higher by $(6\pm4)\%$ in the grain boundary spectrum compared with the nearby bulk. An increase of the L_3/L_2 intensity ratio by $(3\pm1)\%$ on the grain boundary was found. The e_g/t_{2g} intensity ratio in the L_3 edge is larger by 9.6% in the grain boundary compared with the bulk.

The bulk O-*K* edge is dominated by four pronounced peaks (cf. Fig. 8 and the Appendix). As compared to the bulk spectrum, the grain boundary spectrum [Fig. 4(c)] shows a less pronounced and broadened first peak and a weaker second peak. Despite the poor signal-to-noise ratio this can be safely stated because we found the effects consistently in all measurements.

3. EELS mapping

There are intrinsic problems with the area and line scan measurements. The area measurement averages over an area which is large compared to the size of the dislocation core. In the line scan each singular measurement is done on an area comparable to the electron probe size (less than 1 nm $\times$1 nm) which is the utmost resolution obtainable in the STEM. However, it may happen that the scan runs not exactly through the dislocation core. In this case the ''dislocation core spectrum'' might still contain considerable bulk

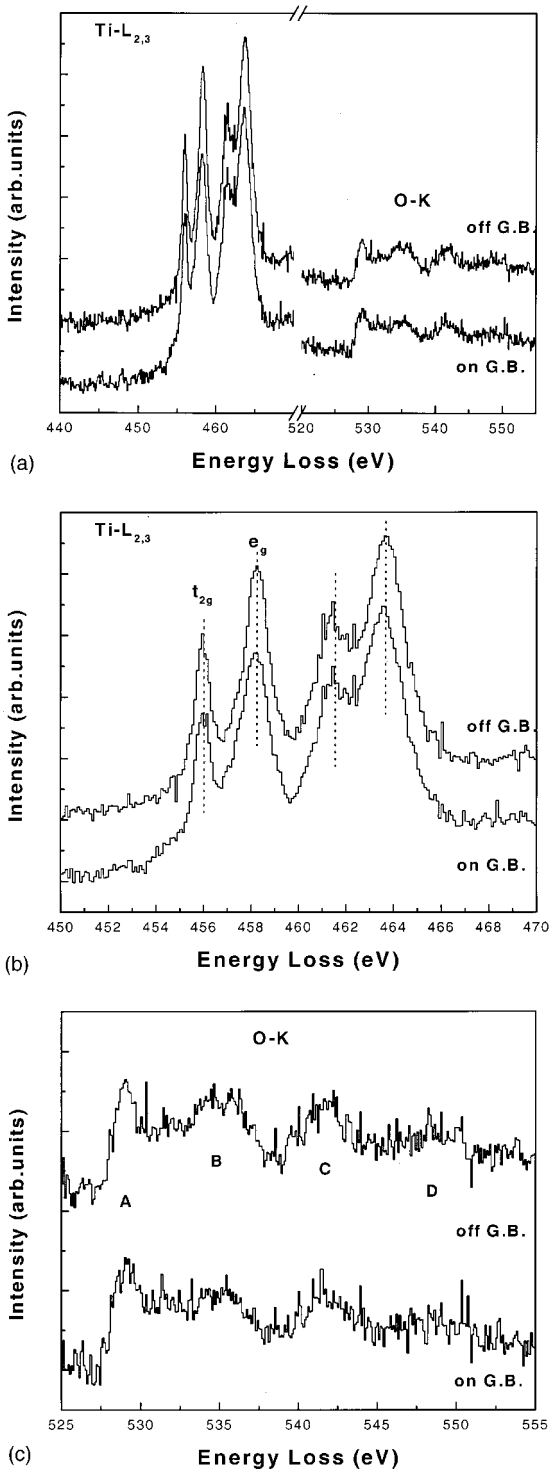

FIG. 4. (a) EELS spectrum from a 1×12 nm area containing three dislocation cores. (b) Enlargement of the Ti-$L_{2,3}$ edge showing a decrease of the crystal-field splitting and a reduced e_g/t_{2g} intensity ratio. (c) Enlargement of the O-*K* edge showing a decrease of peak *B*.

contributions. These drawbacks can be overcome by using the EELS mapping technique. We recorded 25 EELS spectra (5×5) from a quadratic area $(3\times3\ \mathrm{nm}^2)$ containing one individual dislocation core schematically indicated in Fig. 2(b). Thus the separation between neighboring measurements was 0.6 nm, i.e., 1.5 unit cells of the $SrTiO_3$ lattice.

The integration time for each spectrum was 2 s. The spectrometer dispersion was 0.1 eV/channel. By comparing images recorded before and after the EELS acquisition we made sure that the dislocation core was always contained within the probed area. This means that one of the spectra must contain primarily dislocation core information. Indeed, from the total 25 spectra we found one spectrum to be different from the others and we assigned this as the dislocation core specific spectrum. The comparison is shown in Fig. 5(a). The quantification shows an increase of the Ti/O ratio by 15 ± 8 % on the dislocation core as compared to the bulk. The Ti-$L_{2,3}$ edge is shown in more detail in Fig. 5(b). By careful inspection one can see a slight decrease of the crystal field splitting at the dislocation core by 0.2–0.3 eV indicated by dotted lines. The L_3/L_2 ratio is increased by 5.6 ± 2.1 % compared to the bulk. The e_g/t_{2g} intensity ratio in the L_3 edge is larger by 16% in the dislocation core than in the bulk. The oxygen *K* edge [Fig. 5(c)] again shows a decrease of the second peak at the dislocation core whereas the first peak is at least as intense as in the bulk spectrum.

As expected, the changes in the EELS spectra are more pronounced in the mapping and line-scan measurements than in the area measurement because smaller volumes are probed and thus the fraction of the dislocation core signal is higher. The tendency of the results is always the same which makes us confident that they are directly related with the dislocation core properties. To summarize, we find the following significant changes of the EELS spectra in the $a\langle100\rangle$ dislocation cores.

(1) The Ti/O ratio is increased by at least 10% in line-scan and mapping measurements.
(2) The crystal field splitting is reduced by 0.2–0.4 eV.
(3) The e_g/t_{2g} ratio is increased.
(4) The L_3/L_2 ratio is increased.
(5) Peak *B* of the oxygen peak is reduced.

IV. DISCUSSION

From the HRTEM image a blurred contrast in the dislocation core region is visible. Nonetheless, by looking at the image under a glancing angle along the [100] direction, one can clearly distinguish two (010) planes inserted at each core. In the perovskite lattice, {100} planes consist of SrO and TiO_2, respectively. These planes can either be terminated by Sr and O columns or by Ti and O columns. Careful inspection of Fig. 1 further shows that the (010) plane containing the dislocation cores runs straight through the image. This means that the inserted planes are not neighboring planes but that there exists an antiphase boundary (APB) of one unit cell length (marked in Fig. 6) between them, i.e., the dislocation is dissociated. Owing to this dissociation, both inserted atom planes have the same chemical composition. If we assume zero net charge of the dislocation cores, there are four possible configurations for such dislocation cores in the perovskite lattice, two for the SrO-terminated planes (*A*,*B*) and two for the TiO_2-terminated planes (*C, D*). These are shown in Fig. 6 together with the nondissociated core. In fact

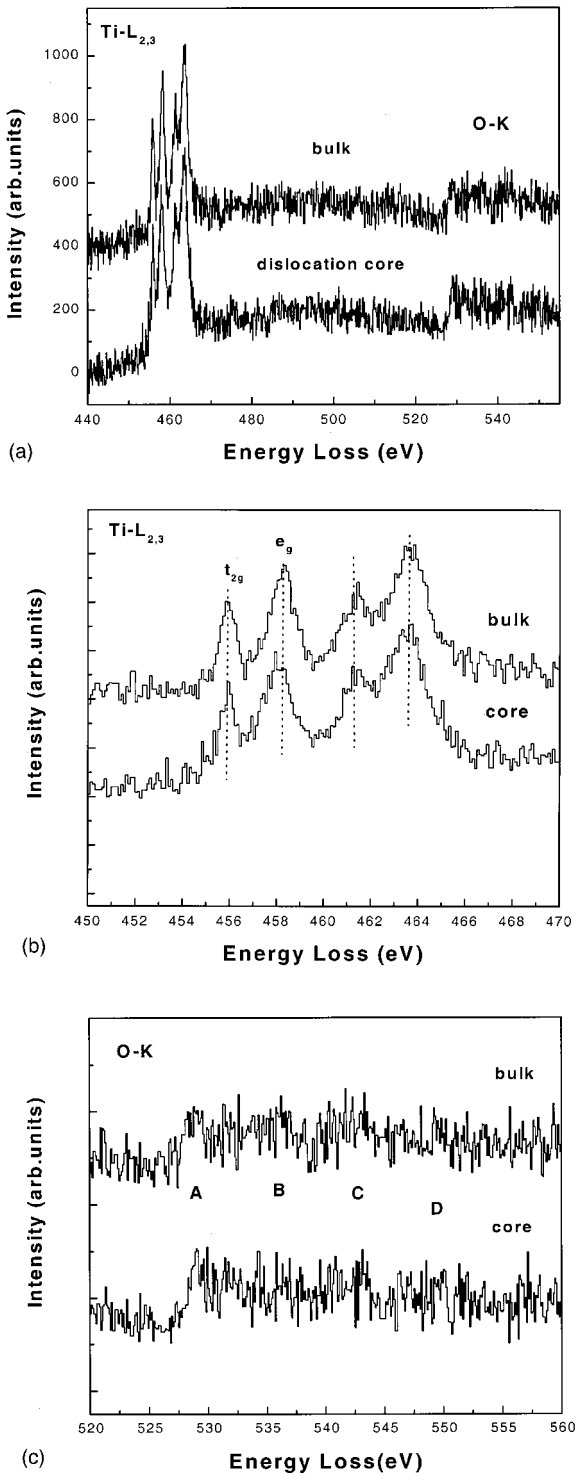

FIG. 5. (a) Two spectra extracted from the EELS map, one in the dislocation core and the other from the surrounding bulk region. (b) Enlargement of the Ti-$L_{2,3}$ edge showing a decrease of the crystal-field splitting. (c) Enlargement of the O-*K*, edge showing a decrease of peak *B*.

a small-angle grain boundary must be composed of at least two core types. In this case four combinations (*..ADAD..,..BCBC..,..ABAB..,..CDCD..*) are possible. The presence of two different core types is corroborated by the fact, that the dislocations marked *a* and *c* in Fig. 1 exhibit a different contrast to dislocations *b* when observed under a glancing angle.

From the EELS results we always found an increase of the Ti/O ratio. The area probed in the EELS line scan and mapping measurements is about 1 by 1 nm^2. By counting the number of atoms within such an area from Fig. 6, we find a Ti/O excess of 4% for cores *C* and *D*, and a Ti/O deficiency of 3.5% for cores *A* and *B*. This deviates from the experimental result. An increase of the Ti/O ratio can be achieved by removing oxygen atoms, by changing the linking of adjacent TiO_x polyhedra, or by allowing for other structural units such as double tetrahedra sharing a face. Unfortunately, from the present HRTEM images it is not possible to make an unambiguous decision. However, the close proximity of O atomic columns in cores *B* and *C* suggests that a more stable structure is achieved by removing one of the oxygen columns. This would lead to the structures shown in Fig. 7 with a Ti/O excess of 4% (*B*) and 13% (*C*) which is closer to the experimental values. For cores *A* and *D*, Ti and Sr atoms are separated by 0.276 nm which is much less than in bulk $SrTiO_3$ (0.338 nm). Therefore, we suppose that these cores are energetically unfavorable. The removal of Ti atoms would lead to a reduction of the Ti/O ratio, in contradiction to our experimental results. The removal of Sr atoms is unlikely, since due to the larger ionic radius the mass transport of Sr atoms in $SrTiO_3$ is difficult. Thus we conclude that the low-angle grain boundary is composed of cores *B* and *C*. An increase of the Ti/O ratio was observed also at grain boundaries[9,20–23] indicating that this may be a general phenomenon near defects in $SrTiO_3$.

By EELS the unoccupied density of states above the Fermi level is probed. The analysis of the energy-loss near-edge structure provides an insight into the local electronic and geometrical structure of the excited atom. The TiO_6 octahedron is an important unit in the $SrTiO_3$ crystal structure. In $SrTiO_3$ adjacent octahedra are connected corner by corner, leading to linear Ti-O-Ti chains along the $\langle 100 \rangle$ directions. The ELNES of the Ti-*L* and O-*K* edges is characteristic for these structural features. Any distortion of the octahedra leads to a change in the ELNES. Such distortions can be expected in the core region of dislocations. An overview of the correlation between the ELNES and the crystal structure is given in the Appendix.

Based on the atomic model shown in Fig. 7, core *B* is composed of distorted corner-shared TiO_6 octahedra, whereas in core *C* two face-shared tetrahedra and one octahedron are connected at a corner. According to Ref. 24, the observed increase of the e_g/t_{2g} intensity ratio and the reduced separation between the e_g and t_{2g} peaks both reflect a reduction of the crystal field. This can be due to a smaller number of nearest oxygen neighbors (such as in the double tetrahedra of core *C*) or to an increase of the Ti-O bond length (which is very likely the case for core *B*). The increase of the Ti/O ratio does certainly not lead to a TiO_2-like structure, since this would lead to a decrease of the e_g/t_{2g} ratio.

The most significant change of the oxygen *K* edge is the reduced intensity of peak *B*. The left shoulder of this peak has been attributed to the e_g peak (from Ti-O $pd\sigma$ bonds),[25] whereas the major part of the peak is related with the Sr-O

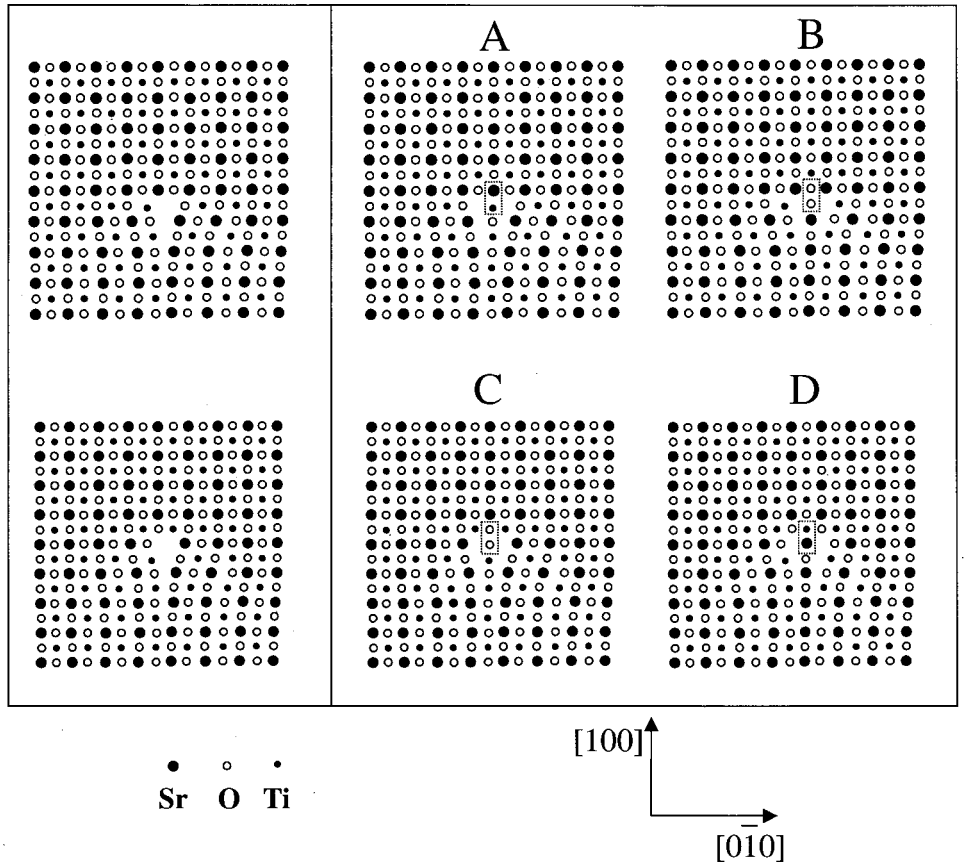

FIG. 6. Four possible atomistic models ($A-D$) for an $a\langle 100\rangle$ dislocation core which is dissociated by half of the lattice parameter. The SrO terminated cores are shown (A,B) on the top, and the TiO-terminated cores (C,D) on the bottom. The cores shown on the left side are the respective nondissociated cores.

bonding.[25–27] A reduced Sr-O bonding is very likely in both cores *B* and *C*. In core *B* this is due to the removal of one O column, whereas in core *C* no Sr atoms are present in the core center.

By the removal of one oxygen column the dislocation core becomes charged by formally two elemental charges per unit cell length. This corresponds closely to the value of $0.93q$ per unit-cell length obtained from impedance spectroscopy performed on the same material.[4] It thus seems that the whole charge is located in the very core of the dislocations.

In a recent study of the plasticity of $SrTiO_3$, it was shown that at elevated temperatures $a\langle 100\rangle$ dislocations have the lowest critical resolved shear stress, whereas at low temperatures $a\langle 110\rangle$ dislocations are more mobile.[5,6] This can be understood from the compact core structure of the $a\langle 100\rangle$ dislocations in Fig. 1. According to the Peierls model, which is likely to be valid at low temperatures, the stress required to move a dislocation increases strongly with decreasing core width. This suggests that the flow stress for $\langle 100\rangle$ glide will be high, at least at low temperatures. A higher mobility could be achieved by a wider core, but this is presumably prevented by a high {100} APB energy. At elevated temperatures dislocation glide can be facilitated by the formation of thermally activated kink pairs.

V. SUMMARY

The combination of HRTEM with EELS provides a perfect tool for the study of the structure and chemistry of dislocation cores in perovskites. In the present study we were able to derive structure models that are consistent not only with our experimental results but also with impedance spectroscopy measurements. Furthermore, by the present results the strong temperature dependence of the mobility of $a\langle 100\rangle$ dislocations can be understood. It is connected with a high {100} APB energy.

In Refs. 5 and 6 it was shown that dislocations with Burgers vector $a\langle 110\rangle$ play a very special role in the plasticity of $SrTiO_3$. Results obtained for these dislocations will be addressed in a forthcoming paper.

ACKNOWLEDGMENTS

One of the authors (Z.L.Z.) is grateful for financial support from the Max-Planck Society. We also thank Maria Sycha for the excellent TEM specimen preparation. We thank Dr. C. Scheu, K. van Benthem, and Dr. G. Richter for helpful discussions and for critically reading the manuscript.

APPENDIX: CORRELATION OF THE ELNES WITH STRUCTURAL FEATURES

1. Ti $L_{2,3}$ edge

The shape of this edge is dominated by four peaks $a-d$ (Fig. 8). These arise from the dipole-allowed excitation of electrons from the inner $2p_{3/2}$ (L_3 edge, peaks *a* and *b*) and $2p_{1/2}$ levels (L_2 edge, peaks *c* and *d*) to the narrow unoccupied $3d$ band, resulting in two narrow peaks (white lines). Both white lines are doubled by the action of the Coulomb field imposed by the surrounding O atoms (crystal-field split-

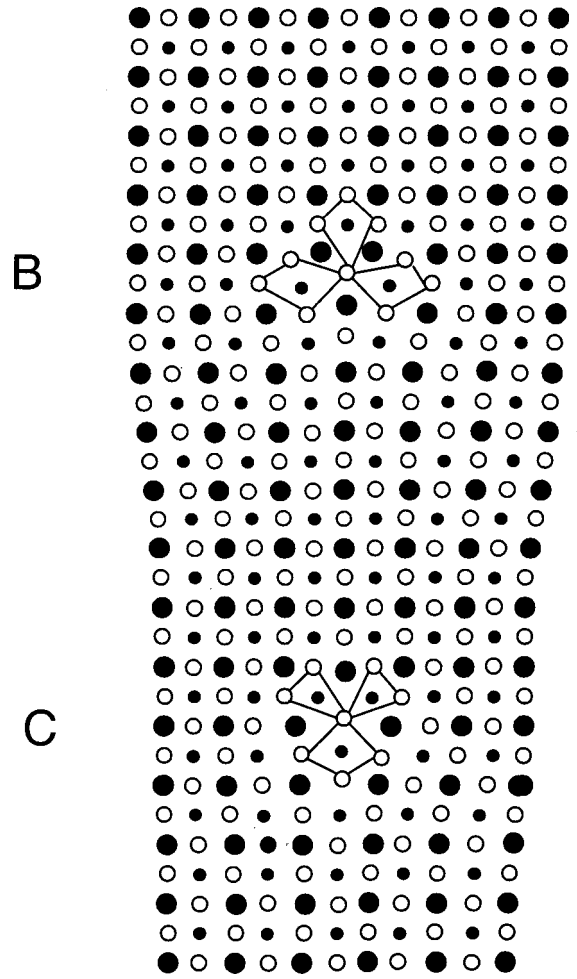

FIG. 7. Structures obtained after reconstruction of cores *B* and *C* (Fig. 6). Compared to Fig. 6 one oxygen column was removed from both cores. This reconstruction leads to a better correspondence of the Ti/O ratio and the e_g/t_{2g} intensity ratio with the experiment.

ting). A perfect octahedral crystal field causes the five degenerate *d* states in the conduction band to split into the twofold e_g orbitals which are directed at the ligands (corresponding to peaks *b* and *d*), and the threefold t_{2g} orbitals which are directed between the ligands (corresponding to peaks *a* and *c*).[28] Whereas a deviation from the octahedral symmetry will create states in the conduction band, a change of the magnitude of the crystal field affects the energetic position and relative intensities of the transitions.[29] However, these changes are generally weak and are often not observable as additional peaks. Rather, a broadening of the white lines or a change of the peak separations is detectable. The $e_g:t_{2g}$ intensity ratio increases and their separation decreases by a reduction of the crystal field.[24] A chemical shift of 1.4 eV toward lower energies is observed in the Ti metal compared to TiO_2.[30] The same authors report a L_3/L_2 ratio of 0.8 for both Ti and TiO_2. The deviation from the statistical ratio of 2:1 (obtained from the $2j+1$ degeneracy of the initial states) is mainly due to the excitation process which leaves a core hole in one of the $2p$ states and an excited electron in the $3d$ band.[31] Taking this into account, Ogasawara *et al.*[32] recently succeeded in approximately reproducing the experimental ratio by nonempirical *ab initio* cluster calculations. By *ab initio* calculations, van Benthem[33] showed that due to the influence of the core hole the measured white line separations deviate from the values in the electronic ground state.

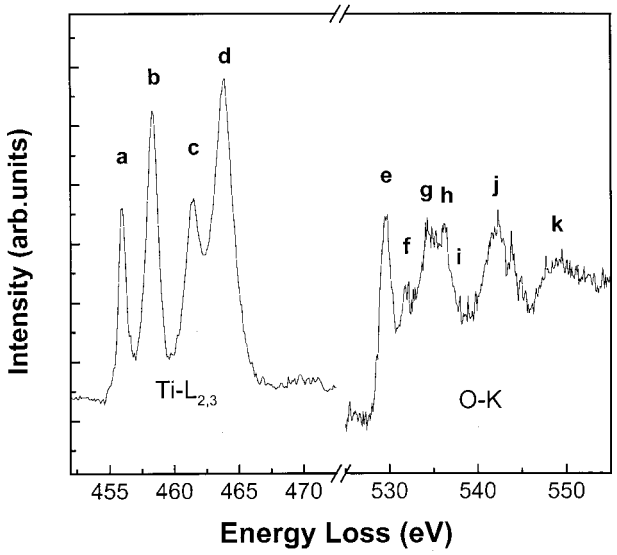

FIG. 8. Typical Ti-$L_{2,3}$ edge and oxygen *K* edge in bulk $SrTiO_3$.

2. Oxygen *K* edge

This edge originates from transitions from the O $1s$ shell to unoccupied $2p$ states and would thus not be visible in a purely ionic compound where all $2p$ states are filled. In transition-metal (TM) oxide compounds, the density of unoccupied oxygen $2p$ states is significantly modified by the strong hybridization with metal $3d$ states. The *O*-K edge in bulk $SrTiO_3$ is shown in Fig. 8. Seven peaks labeled $e-k$ are visible. It is quite generally accepted that peaks *e* and *f* are correlated with the interaction of the oxygen atom with the two nearest-neighbor Ti atoms. *e* can be correlated with the Ti t_{2g} orbital and *f* with the Ti e_g orbital. Brydson *et al.*[26] made the point that a large e/f intensity ratio is typical for a linear chain of Ti-O-Ti tight bonds, as it is the case in $SrTiO_3$. Any distortion of this linearity increases the intensity of *f*. For tetrahedral coordination, like in TiO_2, both peaks have similar intensities.[26,27] By comparing different TM oxides, de Groot *et al.*[34] concluded that the total intensity of *e* and *f* is inversely proportional to the *d*-band filling and thus to the covalency of the Ti-O bonding. The weakness of peak *f* has also been attributed to its broadening by the strong e_g-e_g interaction.[25,27] It is argued that this interaction even leads to a splitting of the e_g band leading to the separate peak *g*. From this Tanaka *et al.*[25] concluded that the e_g intensity and the separation of *f* and *g* should sensitively depend on the Ti-O bonding angle. Peaks *h* and *i* most probably are related with the Sr-O bonding.[25–27] There is no unambiguous assignment of peak *j* to structural features. Whereas de Groot *et al.*[27] assumed this peak to originate from the Sr $4p$ band, Tanaka *et al.* assigned it to the Ti $4s$ band. Finally,

peak *k* is generally assumed to be related with the Ti 4*p* band. Wallis and Browning[35] and Browning, Moltaji and Buban[36] performed multiple-scattering calculations using clusters extracted from the perovskite structure. By removing atoms from the cluster they assigned spectral to structural features. Apart from peaks *e* and *f*, they assigned the other peaks mainly to the scattering from the surrounding oxygen atoms.

[1] W. Heywang, J. Am. Ceram. Soc. **47**, 484 (1964).
[2] A. I. Kingon, E. R. Myers, and B. Tuttle, *Ferroelectric Thin films II*, MRS Symposia Proceedings No. 243 (Materials Research Society, Pittsburgh, 1991).
[3] Y.-M. Chiang, D. P. Birnie, and W. D. Kingery, *Electro Ceramics* (Wiley, New York, 1997).
[4] R. A. de Souza, J. Fleig, J. Maier, O. Kienzle, Z. L. Zhang, W. Sigle, and M. Rühle (unpublished).
[5] D. Brunner, S. Taeri-Baghbadrani, W. Sigle, and M. Rühle, J. Am. Ceram. Soc. **84**, 1161 (2001).
[6] P. Gumbsch, S. Taeri-Baghbadrani, D. Brunner, W. Sigle, and M. Rühle, Phys. Rev. Lett. **87**, 085505 (2001).
[7] R. Brydson, J. Bruley, H. Müllejans, C. Scheu, and M. Rühle, Ultramicroscopy **59**, 81 (1995).
[8] C. Scheu and W. Stein, M. Rühle, Phys. Status Solidi B **222**, 199B (2000).
[9] H. Müllejans and J. Bruley, J. Microsc. **180**, 12 (1995).
[10] S. Nufer, A. G. Marinopoulos, T. Gemming, C. Elsässer, W. Kurtz, S. Köstlmeier, and M. Rühle, Phys. Rev. Lett. **86**, 5066 (2001).
[11] H. Gu, M. Čeh, S. Stemmer, H. Müllejans, and M. Rühle, Ultramicroscopy **59**, 215 (1995).
[12] P. E. Batson, Phys. Rev. B **61**, 16 633 (2000).
[13] Y. Xin, E. M. James, I. Arslan, S. Sivananthan, N. D. Browning, S. J. Pennycook, F. Omnes, B. Beaumont, J-P. Faurie, and P. Gibart, Appl. Phys. Lett. **76**, 466 (2000).
[14] S. Hutt, O. Kienzle, F. Ernst, and M. Rühle, Z. Metallkd. **92**, 105 (2001).
[15] A. Strecker, U. Salzberger, and J. Mayer, Prakt. Metallogr. **30**, 482 (1993).
[16] R. F. Egerton, *Electron Energy Loss Spectroscopy in the Electron Microscope*, 2nd ed. (Plenum, New York, 1996).
[17] D. H. Pearson, C. C. Ahn, and B. Fultz, Phys. Rev. B **47**, 8471 (1993).
[18] V. E. Heinrich, G. Dresselhaus, and H. J. Zeiger, Phys. Rev. B **17**, 4908 (1978).
[19] G. Möbus, Ultramicroscopy **65**, 205 (1996).
[20] S. Stemmer, S. K. Streiffer, N. D. Browning, C. Basceri, and A. I. Kingon, Interface Sci. **8**, 209 (2000).
[21] G. Duscher, J. P. Buban, N. D. Browning, M. F. Chisholm, and S. J. Pennycook, Interface Sci. **8**, 199 (2000).
[22] K. van Benthem, R. H. French, W. Sigle, C. Elsässer, and M. Rühle, Ultramicroscopy **86**, 303 (2001).
[23] M. Y. Kim, G. Duscher, N. D. Browning, K. Sohlberg, S. T. Pantelides, and S. J. Pennycook, Phys. Rev. Lett. **86**, 4056 (2001).
[24] G. van der Laan and I. W. Kirkman, J. Phys.: Condens. Matter **4**, 4189 (1992).
[25] I. Tanaka, T. Nakajima, J. Kawai, H. Adachi, H. Gu, and M. Rühle, Philos. Mag. Lett. **75**, 21 (1997).
[26] R. Brydson, H. Sauer, W. Engel, and F. Hofer, J. Phys.: Condens. Matter **4**, 3429 (1992).
[27] F. M. F. de Groot, J. Faber, J. J. M. Michiels, M. T. Czyzyk, M. Abbate, and J. C. Fuggle, Phys. Rev. B **48**, 2074 (1993).
[28] R. J. Bong and G. J. Dienes, *The Physical Chemistry of Solids* (Academic, New York, 1992), pp. 179–227.
[29] R. Brydson, L. A. J. Garvie, A. J. Craven, H. Sauer, F. Hofer, and G. Cressey, J. Phys.: Condens. Matter **5**, 9379 (1993).
[30] R. D. Leapman, L. A. Grunes, and P. L. Fejes, Phys. Rev. B **26**, 614 (1982).
[31] W. G. Waddington, P. Rez, I. P. Grant, and C. J. Humphreys, Phys. Rev. B **34**, 1467 (1986).
[32] K. Ogasawara, T. Iwata, Y. Koyama, T. Ishii, I. Tanaka, and H. Adachi, Phys. Rev. B **64**, 115413 (2001).
[33] K. van Benthem, Ph.D. thesis, Universität Stuttgart, 2002.
[34] F. M. F. de Groot, M. Grioni, J. C. Fuggle, J. Ghijsen, G. A. Sawatzky, and H. Petersen, Phys. Rev. B **40**, 5715 (1989).
[35] D. J. Wallis and N. D. Browning, J. Am. Ceram. Soc. **80**, 781 (1997).
[36] N. D. Browning, H. O. Moltaji, and J. P. Buban, Phys. Rev. B **58**, 8289 (1998).